



# Mechanical and Thermal Oxidation Behavior of Poly(Lactic Acid)/Halloysite Nanotube Nanocomposites Containing *N,N'*-Ethylenebis(Stearamide) and SEBS-g-MA

W. S. Chow<sup>1</sup> · W. L. Tham<sup>1</sup> · B. T. Poh<sup>2</sup> · Z. A. Mohd Ishak<sup>1</sup>

Published online: 27 January 2018

© Springer Science+Business Media, LLC, part of Springer Nature 2018

## Abstract

Poly(lactic acid) (PLA)/halloysite nanotube (HNT) nanocomposites were prepared using melt compounding followed by compression molding. Maleic anhydride grafted styrene–ethylene/butylene–styrene copolymer (SEBS-g-MA) and *N,N'*-ethylenebis(stearamide) (EBS) were used to improve the impact properties of PLA nanocomposites. The properties of PLA/HNT nanocomposites were characterized by tensile and impact tests, Fourier transform infrared spectroscopy, thermal analysis (DSC and TGA), and morphological analysis (FESEM and TEM). In addition, the oxidation onset temperature (OOT) was determined using DSC. The PLA/HNT6/EBS5 nanocomposites gives higher impact strength improvement (98%) compared to that of PLA/HNT6/SEBS-g-MA5 (77%). Also, the PLA/HNT6/EBS5 exhibited higher OOT compared to that of PLA/HNT6/SEBS-g-MA5 nanocomposites.

**Keywords** Poly(lactic acid) · Halloysite · Maleic anhydride grafted styrene–ethylene/butylene–styrene copolymer · *N,N'*-ethylenebis(stearamide) · Oxidation onset temperature

## Introduction

Polymer nanocomposites have attracted great attention worldwide from both academic and industries. The properties of polymer can be enhanced by incorporating nanofillers at very low concentrations [1]. The enhanced properties of polymer nanocomposites are attributed to the nanoscale structure, the large aspect ratio of the nanofiller and the strong interaction between polymer molecular chains and nanofiller [2, 3]. Poly(lactic acid) (PLA) is an attractive biopolymer due to its sustainability and eco-friendly which are derived from the renewable resources, e.g. corn, sugar beets, and sugarcane. PLA offers good mechanical properties (i.e. high strength and modulus), good thermal

processability, transparency, biodegradability, and biocompatibility [4–8].

Halloysite nanotubes (HNT) have recently received increasing research attention due to the combination of the chemistry of montmorillonite and the geometry of carbon nanotubes. The HNT is similar to the kaolin group of clay minerals with the chemical composition of  $\text{Al}_2(\text{OH})_4\text{Si}_2\text{O}_5(2\text{H}_2\text{O})$ . It exhibits hollow nanotubular structure and its typical dimension is of nanoscale with high aspect ratio. Furthermore, the cost of HNT is far cheaper than other nanofillers such as carbon nanotubes [9, 10]. In this research, HNT was incorporated in the PLA matrix in order to produce a green nanocomposite, with the intention of obtaining materials with improved properties which is suitable for a wide range of applications. The incorporation of HNT could improve the properties of polymer matrix in terms of mechanical, fire retardant, rheological, and gas barrier properties [11–13].

The applications of PLA are limited by several factors such as low glass transition temperature, low thermal resistance and brittle. PLA has been blended with others polymers for toughness improvement, e.g., poly[(3-hydroxybutyrate)-co-(3-hydroxyhexanoate)] [14], poly(acrylic acid) and poly(ethylene glycol) [15], polyhydroxyalkanoates [16],

✉ W. S. Chow  
shyang@usm.my

<sup>1</sup> School of Materials and Mineral Resources Engineering, Universiti Sains Malaysia, Engineering Campus, 14300 Penang, Malaysia

<sup>2</sup> School of Industrial Technology, Universiti Sains Malaysia, 11800 Penang, Malaysia

polyethylene octane grafted maleic anhydride (MA) [17] and poly(butylenes succinate) [18].

In this study, SEBS-g-MA and EBS have been selected as an attempt to improve the impact properties of PLA nanocomposites. The SEBS is a styrenic block polymer consisting of polystyrene blocks and rubber blocks. The rubber block consists of ethylene/butylenes (EB) is efficient to act as bumpers that absorb the impact energy and also play as crack initiator stops in polymer system. MA can be grafted to the EB chain to improve the properties of polymers, by providing polarity to enhance the adhesion and compatibility with other polymers and fillers [19, 20]. It is known that SEBS-g-MA is a common rubbery polymer which has been used as impact modifiers and compatibilizer to improve the toughness for certain polymer composites [21–24].

The *N,N'*-ethylenebis(stearamide) (EBS) has low molecular weight and flexible hydrocarbon segment with the existence of polar amide groups (–CONH–) in the molecular structure of EBS make it compatible with some of the polar polymer. Several articles reported that EBS can act as a lubricant and plasticizer in HDPE/bark fiber composites [25], polyethylene/maple composites [26], PE/cassava starch [27], high impact polystyrene/magnesium hydroxide [28], and poly(3-hydroxybutyrate-*co*-4-hydroxybutyrate)/short glass fiber composites [29].

In this paper, we aim to report the effects of SEBS-g-MA and EBS on the mechanical and thermal properties of PLA/HNT nanocomposites. It is known that SEBS-g-MA could act as impact modifier for polymer composites (and/or nanocomposites). Hence, comparative studies were done on both PLA/HNT/SEBS-g-MA and PLA/HNT/EBS, in order to check the feasibility of EBS to be used as impact modifier for PLA/HNT nanocomposites. At the same time, the thermal oxidation behaviours of the PLA/HNT nanocomposites were evaluated.

## Experimental

### Materials

PLA (Ingeo™ 3051D, NatureWorks LLC®, USA) was selected in this study. The specific gravity and melt flow index of the PLA were 1.25 g cm<sup>-3</sup> and 25 g 10 min<sup>-1</sup> (2.16 kg load, 210 °C), respectively. HNT was supplied by Sigma-Aldrich (Malaysia). The diameter of the HNT was in the range of 30–70 nm, while its length was 1–3 μm. SEBS-g-MA, with a MA grafting level of 1.4–2.0 wt% and styrene/rubber ratio of 30/70 (wt%), was purchased from Shanghai Jianqiao Plastic Co. Ltd., (China). The melt flow index and specific gravity of the SEBS-g-MA were 1.0 g 10 min<sup>-1</sup> (2.16 kg load, 230 °C) and 0.91 g cm<sup>-3</sup>, respectively. EBS was supplied by Sigma-Aldrich (USA). The melting point and density of EBS is 140 °C and 0.97 g cm<sup>-3</sup>, respectively. The molecular weight of EBS is 593 g mol<sup>-1</sup>.

### Preparation of PLA/HNT Nanocomposites

Melt compounding was carried out by using an internal mixer (Haake PolyDrive R600, Germany) at 180 °C for 10 min. The rotor speed was set at 50 rpm. Prior to compounding, PLA, HNT, SEBS-g-MA and EBS were dehumidified in a vacuum oven at 80 °C for 24 h. During compounding, the HNTs were mixed with PLA, followed by the addition of SEBS-g-MA or EBS. Table 1 shows the materials designations and compositions for PLA/HNT6 nanocomposites. The compression molding was performed at 185 °C using a hot press machine (Go Tech, Taiwan). The preheating, compression molding and cooling times were 7, 3, and 3 min, respectively.

**Table 1** Materials designations and compositions of PLA/HNT6 nanocomposites

Materials designation	PLA (wt%)	HNT (wt%)	SEBS-g-MA (wt%)	EBS (wt%)
PLA	100	–	–	–
PLA/HNT6	94	6	–	–
PLA/HNT6/SEBS-g-MA5	89	6	5	–
PLA/HNT6/SEBS-g-MA10	84	6	10	–
PLA/HNT6/SEBS-g-MA15	79	6	15	–
PLA/HNT6/SEBS-g-MA20	74	6	20	–
PLA/HNT6/EBS5	89	6	–	5
PLA/HNT6/EBS10	84	6	–	10
PLA/HNT6/EBS15	79	6	–	15
PLA/HNT6/EBS20	74	6	–	20

## Characterization of PLA/HNT Nanocomposites

### Mechanical Properties

Tensile tests were carried out on an Instron tensile machine (model 3366, USA) at 27 °C and 50% relative humidity, according to ASTM D638. Tensile modulus, tensile strength and elongation at break were determined from the stress–strain curves. The Charpy impact strength of the samples was determined according to ASTM D6110 by using a pendulum impact machine (model 5101, Zwick, Germany). The dimension of sample was 65 mm × 13 mm × 3 mm (length × width × thickness). The testing was performed with pendulum of 7.5 J with a velocity of 3.54 m s<sup>-1</sup>.

### Field Emission Scanning Electron Microscopy (FESEM)

The fracture surfaces of selected PLA nanocomposites were investigated in a FESEM (Zeiss Supra 35VP, Germany) at an acceleration voltage of 5 kV. The specimen surfaces were gold coated to avoid electrostatic charging during examination.

### Transmission Electron Microscopy (TEM)

PLA specimens (approximately 50 nm) were prepared using a PT-PC PowerTome ultramicrotome (Boeckeler Instruments, Arizona, USA) with a diatome diamond knife. The PLA specimens were stained using osmium tetroxide (OsO<sub>4</sub>) to provide contrast to the image. TEM viewing was then performed using a Zeiss Libra 120 Plus energy filtering transmission electron microscope (Carl Zeiss, Germany) operating at an accelerating voltage of 120 kV.

### Fourier Transform Infrared Spectroscopy (FTIR)

FTIR spectrophotometer (Perkin Elmer Spectrum One, UK) was used to characterize the functional group of PLA/HNT nanocomposites. FTIR spectra were determined from 400 to 4000 cm<sup>-1</sup> with a resolution of 4 cm<sup>-1</sup>.

### Thermogravimetric Analysis (TGA)

Thermal decomposition behaviour of the PLA samples was characterized by using a thermogravimetric analyzer (TGA, Perkin Elmer Pyris 6, USA). The TGA was performed in both nitrogen and oxygen atmosphere. In both measurements, the samples were heated from 30 to 600 °C at a heating rate of 10 °C min<sup>-1</sup>.

### Differential Scanning Calorimetry (DSC)

The melting and crystallization behaviour of the composites were scanned under nitrogen atmosphere by DSC 1 (Mettler Toledo STAR<sup>®</sup>, USA) using approximately 10 mg samples sealed in aluminum pans. The specimens were scanned from 30 to 200 °C at a heating rate of 10 °C min<sup>-1</sup>. The glass transition temperature (*T<sub>g</sub>*), melting temperature (*T<sub>m</sub>*), cold crystallization temperature (*T<sub>cc</sub>*) and degree of crystallinity (*χ<sub>c</sub>*) of the PLA nanocomposites were determined. The degree of crystallinity (*χ<sub>c</sub>*) of PLA nanocomposites was evaluated according to Eq. (1).

$$\chi_c = \frac{\Delta H_m}{\Delta H_f \times w_{PLA}} \times 100\% \quad (1)$$

where  $\Delta H_m$  is the enthalpy of melting;  $\Delta H_f$  is the enthalpy for 100% crystalline PLA, and  $w_{PLA}$  is the net weight fraction of the PLA. The heat of fusion for 100% crystalline PLA is approximately 93.6 J g<sup>-1</sup> [30, 31].

### Oxidation Onset Temperature (OOT)

The OOT was determined using differential scanning calorimetry (DSC Q200, TA instruments, USA). The samples (10 mg) in opened Tzero pan were heated at heating rate of 10 °C min<sup>-1</sup> up to 180 °C under nitrogen atmosphere (50 mL min<sup>-1</sup>) and isothermal for 2 min. The atmosphere was then switched from nitrogen to oxygen atmosphere. The flow rate of O<sub>2</sub> gas was set at 50 mL min<sup>-1</sup>, and then heated up from 180 °C until the OOT occurred.

## Results and Discussion

### Mechanical Properties

Table 2 shows the tensile and impact properties of PLA/HNT6 nanocomposites. The tensile modulus of PLA was increased with the addition of 6 wt% HNT. The improvement of tensile modulus is attributed to the rigidity and reinforcing-ability of HNT. It can be observed that the addition of SEBS-g-MA and EBS into PLA nanocomposites decreases the tensile modulus and strength due to the elastomeric nature of the impact modifier. It is worth to mention that the tensile modulus of PLA/HNT6 containing EBS is higher than that of PLA/HNT6/SEBS-g-MA. The elongation at break of PLA was decreased in the presence of HNT. This may be due to the constraint of mobility on the polymer chains caused by the HNT. Nevertheless, the incorporation of SEBS-g-MA into PLA/HNT nanocomposites increased the elongation at break. It is suggested that SEBS-g-MA is capable of inducing an energy dissipation mechanism in

**Table 2** Effects of SEBS-g-MA and EBS on the mechanical properties of PLA/HNT6 nanocomposites

Materials designation	Tensile modulus (GPa)	Tensile strength (MPa)	Elongation at break (%)	Impact strength ( $\text{kJ m}^{-2}$ )
PLA	$1.7 \pm 0.10$	$60.0 \pm 1.4$	$4.6 \pm 0.7$	$9.0 \pm 0.7$
PLA/HNT6	$2.0 \pm 0.04$	$49.5 \pm 0.7$	$3.8 \pm 0.2$	$11.4 \pm 1.4$
PLA/HNT6/SEBS-g-MA5	$1.8 \pm 0.09$	$39.1 \pm 2.0$	$3.8 \pm 0.2$	$20.2 \pm 1.9$
PLA/HNT6/SEBS-g-MA10	$1.5 \pm 0.05$	$33.9 \pm 1.4$	$4.1 \pm 0.2$	$19.7 \pm 2.2$
PLA/HNT6/SEBS-g-MA15	$1.2 \pm 0.08$	$28.7 \pm 0.6$	$4.7 \pm 0.2$	$16.4 \pm 1.4$
PLA/HNT6/SEBS-g-MA20	$1.1 \pm 0.06$	$24.1 \pm 0.6$	$5.1 \pm 0.5$	$16.6 \pm 1.8$
PLA/HNT6/EBS5	$1.6 \pm 0.06$	$38.4 \pm 1.1$	$3.5 \pm 0.2$	$22.6 \pm 1.2$
PLA/HNT6/EBS10	$1.7 \pm 0.09$	$35.4 \pm 2.2$	$3.3 \pm 0.3$	$17.9 \pm 1.8$
PLA/HNT6/EBS15	$1.7 \pm 0.04$	$29.1 \pm 2.9$	$3.6 \pm 0.3$	$15.3 \pm 2.3$
PLA/HNT6/EBS20	$2.0 \pm 0.02$	$26.1 \pm 0.9$	$3.1 \pm 0.3$	$13.9 \pm 1.1$

the PLA composites and may elongate to a greater extent, avoiding a highly strained process during the tensile deformation. On the other hand, the elongation at break of PLA/HNT6 containing EBS is in the range of 3.1–3.6% which is comparable with the PLA/HNT6 nanocomposites.

The incorporation of 6 wt% HNT increases the impact strength of PLA to approximately  $11.4 \text{ kJ m}^{-2}$ . The inorganic particles act as stress concentrator to build up a stress field surrounded polymer matrix. The debonding of inorganic particle occurs at the particle–matrix interface would take place, leading to the release of the strain constraints at the crack tip. Thus, it may cause the plastic deformation to dissipate a large amount of energy [32–35]. The addition of 5 wt% SEBS-g-MA and 5 wt% EBS increased the impact strength of the PLA/HNT6 to approximately 77 and 98%, respectively. Again, this is attributed to the elastomeric nature of the SEBS-g-MA which can induce higher energy absorption during an impact test and give higher impact strength for the PLA/HNT nanocomposites. According to Bartczak et al. [36], the cavitation of rubber particles is a main mechanism to increase polymer toughness due to energy dissipation. Note that the addition of 5 wt% EBS in PLA/HNT6 gives higher impact strength compared to that of PLA/HNT6 containing 5 wt% SEBS-g-MA. This may due to EBS can act as a dispersant for the HNT in PLA matrix [32].

### Fourier Transform Infrared Spectroscopy

Figure 1 shows the FTIR spectra of PLA/HNT6 with and without SEBS-g-MA. The new bands appeared at 2924 and  $2852 \text{ cm}^{-1}$  for the PLA/HNT6/SEBS-g-MA nanocomposites can be assigned to the C–H stretching and  $-\text{CH}_2$  group from SEBS-g-MA. Additionally, the band intensity of 2924 and  $2852 \text{ cm}^{-1}$  is more noticeable as the SEBS-g-MA loading increased to 20 wt%. Note that the peak at  $3503 \text{ cm}^{-1}$  was shifted to  $3487 \text{ cm}^{-1}$  as the increasing of SEBS-g-MA loading. These peaks were attributed to the O–H stretching

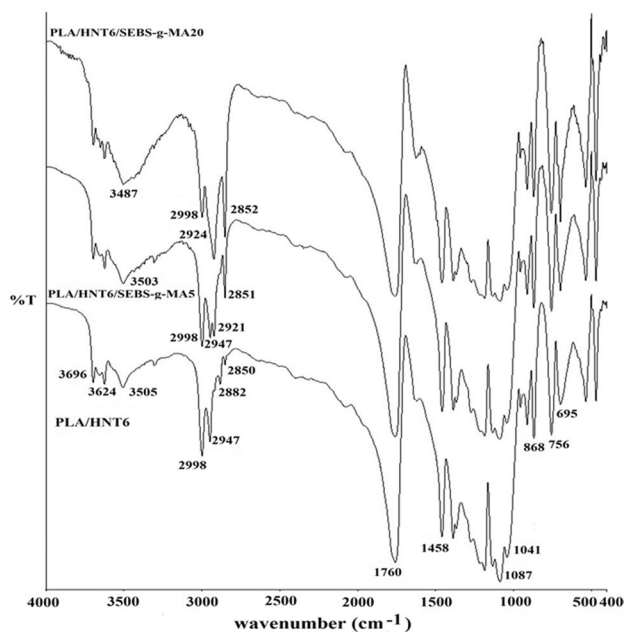


**Fig. 1** FTIR spectra of PLA/HNT6, PLA/HNT6/SEBS-g-MA5, and PLA/HNT6/SEBS-g-MA20 nanocomposites

from the hydrogen bonding of water molecules or lateral groups of amino acids, such as protonated carboxylic acids. The intensity peak at  $3487 \text{ cm}^{-1}$  becomes more obvious as the SEBS-g-MA loading increases to 20 wt%, which indicates the better interaction between MA and Si–O group. Figure 2 shows the FTIR spectra of PLA/HNT6, PLA/HNT6/EBS5, and PLA/HNT6/EBS20 nanocomposites. The new peaks at 3300, 1639, and  $1556 \text{ cm}^{-1}$  have appeared in the FTIR spectra of PLA/HNT6 in the presence of EBS. The peaks at 3300 and  $1639 \text{ cm}^{-1}$  is associated to N–H stretching, while the absorption band at  $1556 \text{ cm}^{-1}$  is assigned to C=O, which are originated from the amide group ( $-\text{CONH}$ ) of EBS. The appearance of peaks at 2919 and  $2850 \text{ cm}^{-1}$  is



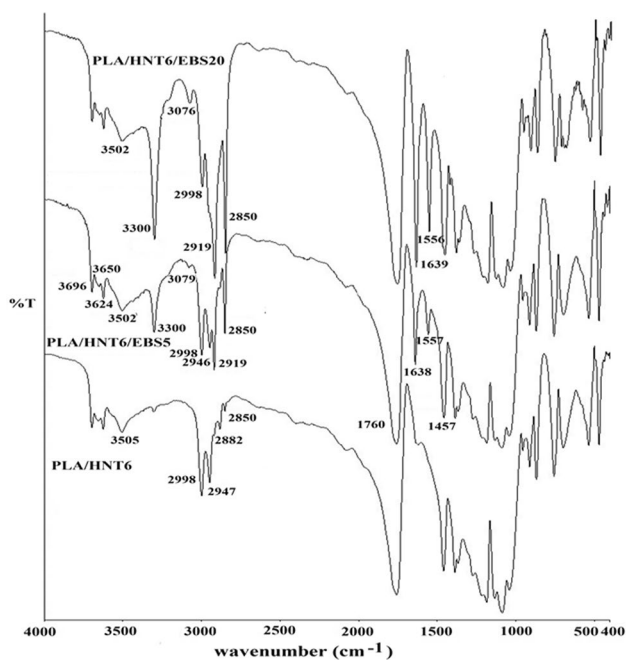


**Fig. 2** FTIR spectra of PLA/HNT6, PLA/HNT6/EBS5, and PLA/HNT6/EBS20 nanocomposites

attributed to the aliphatic C–H group of EBS as the loading of EBS increased. The presence of amide group in EBS can lead to inter- and/or intra-molecular reaction between each

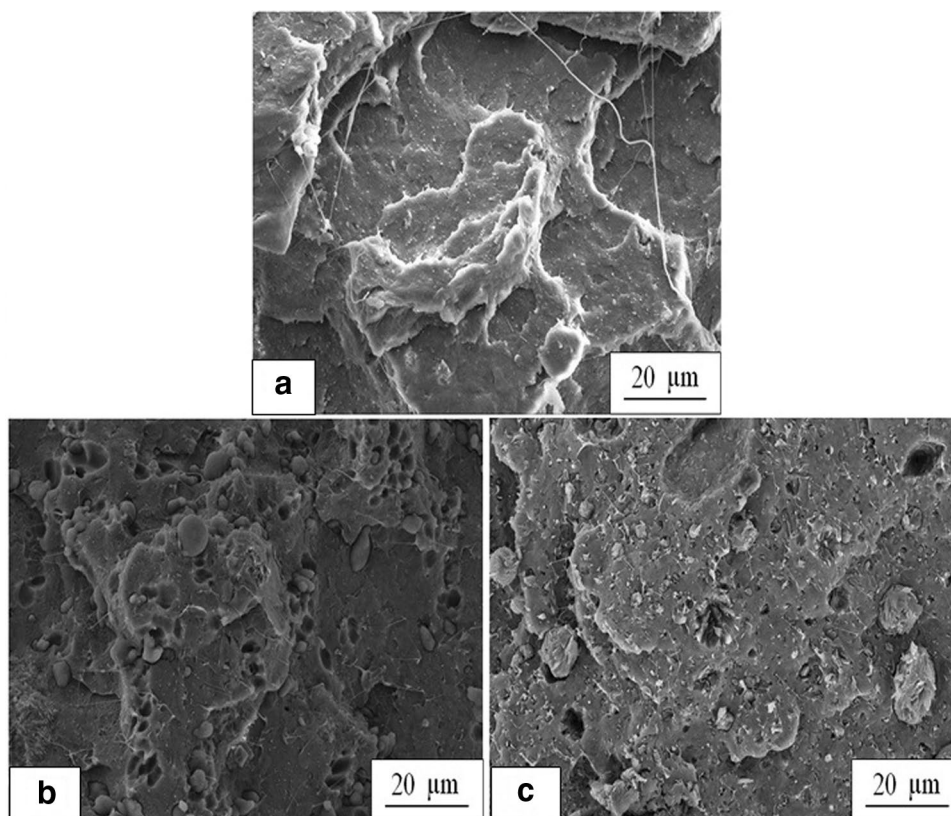
other to form hydrogen bonding. There are also possibility for the chemical interaction between C=O from PLA and hydroxyl group from HNT with the amide group of EBS.

### Field Emission Scanning Electron Microscopy (FESEM)

Figure 3 shows FESEM micrographs taken from impact fracture surfaces of PLA nanocomposites. The formation of non-planar fracture surfaces and plastic deformation in PLA/HNT6 can be observed in Fig. 3a. A relatively rough fracture surface and crack fronts on the fracture surface of PLA/HNT6 was observed. It was suggested that a crack path deflection due to the rigidness of HNT hindered crack propagation, and thus more energy dissipated during the fracture mechanism [37]. Therefore, HNT could improve impact strength of PLA.

Figure 3b, c shows a more extensive plastic deformation and rougher surface were observed on the fracture surface of PLA/HNT containing impact modifiers (i.e. SEBS-g-MA and EBS). The FESEM micrograph of PLA/HNT6/SEBS-g-MA5 (c.f. Fig. 3b) contains smooth and distinct droplets protruded on the PLA fracture surface, indicating that the SEBS-g-MA particles are not miscible with PLA matrix and have less interfacial adhesion. The microcavities were observed on the impact fracture surface of PLA/HNT6/SEBS-g-MA5, which corresponded to the

**Fig. 3** FESEM micrographs taken from impact fracture surfaces of **a** PLA/HNT6, **b** PLA/HNT6/SEBS-g-MA5, and **c** PLA/HNT6/EBS5



SEBS-g-MA particles detached from the PLA matrix surface. The cavitations associated with localized shear band formation proceeded crazing in the sample. The crazing is commonly controlled by the foreign particles, which act as stress concentrators. The rubber-modified polymer acts as stress concentrators due to the formation of a large number of crazes distributed throughout the sample volumes. From Fig. 3c, it can be observed that the EBS is mostly embedded on the fracture surface of PLA nanocomposites, indicating a good interaction/adhesion between HNT, EBS and PLA. The EBS with particle size 1–2  $\mu\text{m}$  was observed on its fracture surface (c.f. Fig. 3c). This morphology can be related to the enhancement in impact strength of PLA/HNT6/EBS5.

### Transmission Electron Microscopy (TEM)

Figure 4 shows the TEM micrographs of the PLA/HNT nanocomposites. In Fig. 4a, b, the dark region with elongated droplet shape was ascribed to the SEBS-g-MA with the dimension of approximately 2–5  $\mu\text{m}$ . It is interesting to note that the HNT appeared in different morphologies with small bundles and single dispersed nanotubes can be observed after the addition of SEBS-g-MA within polymer. The occurrence of different sizes, broken and folded

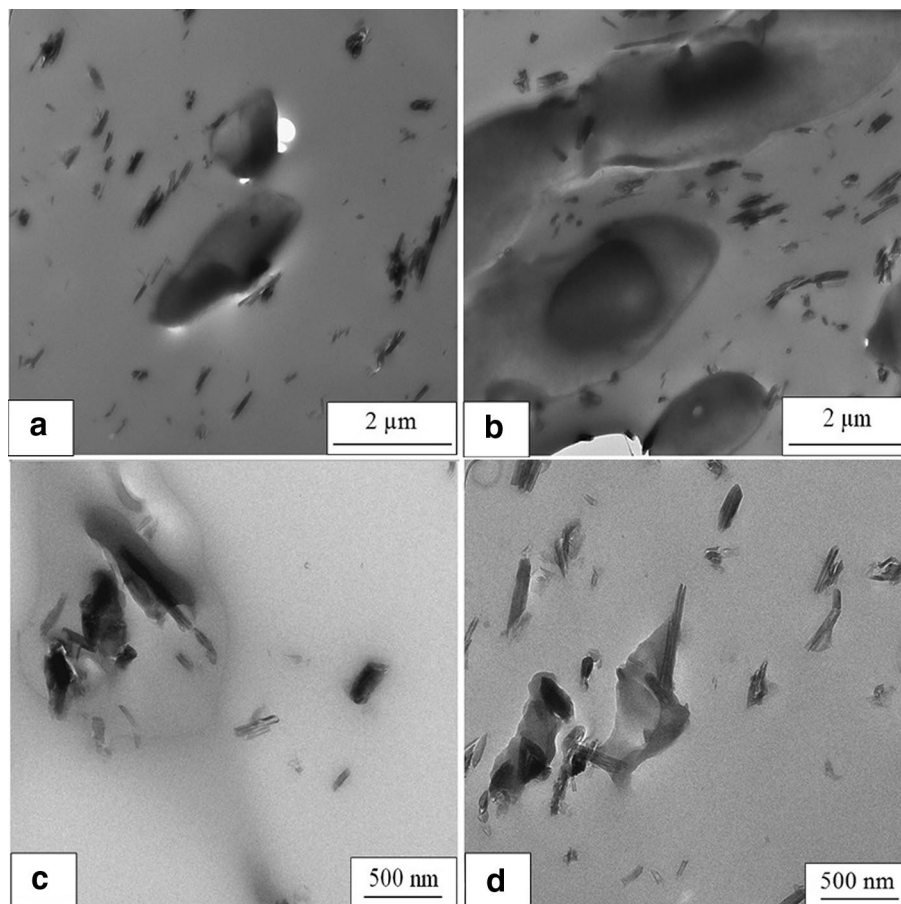
nanotubes of HNT may be due to the existence of a benzene group of SEBS-g-MA which restrict the dispersion of HNT, probably resulting from mechanical damage during the mixing process, which caused the breakage of the HNT nanotubular.

Figure 4c, d shows the TEM images of PLA/HNT nanocomposites containing 5 and 20 wt% EBS. The dark region with irregular shape can be ascribed to EBS. It can be observed that the dimension of EBS is about 0.5–1  $\mu\text{m}$ . The EBS promotes better dispersion of HNT in PLA matrix. It can be seen that the HNT are mainly located at the surface of EBS, thus suggesting a strong affinity by the formation of hydrogen bonding between the surface OH groups of HNT and amide group of EBS.

### Thermogravimetric Analysis (TGA)

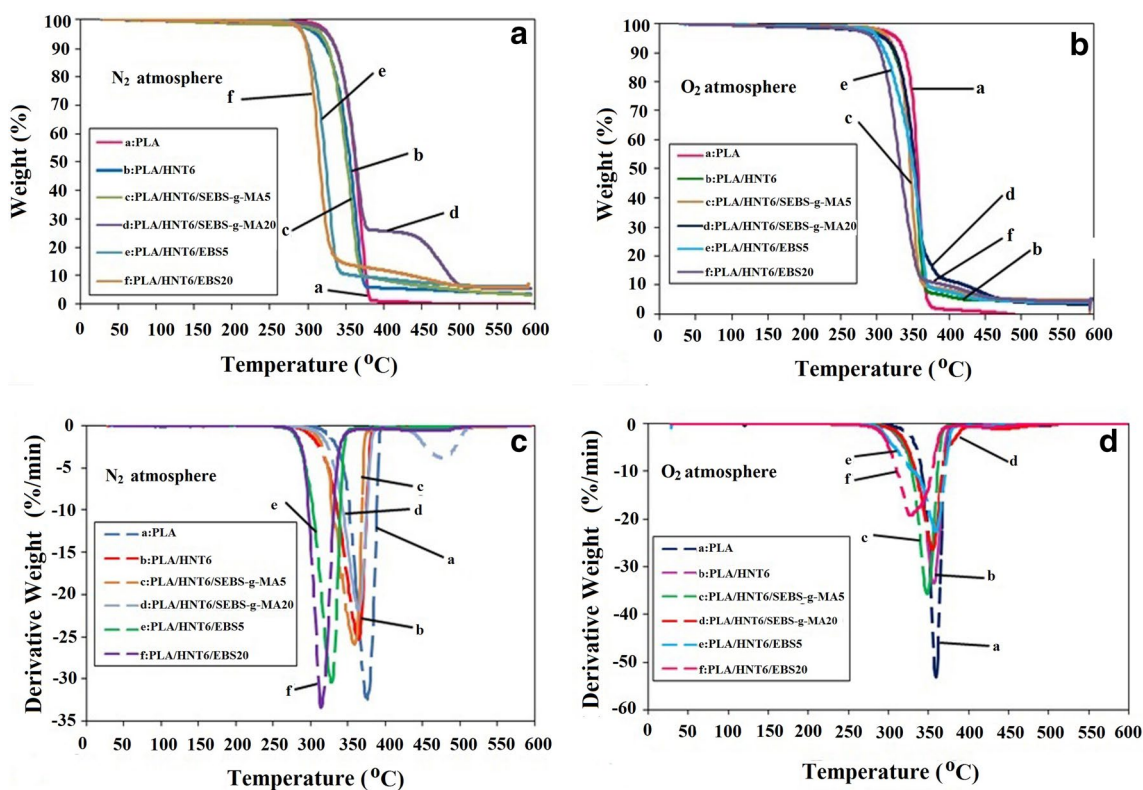
Table 3 summarises the thermal decomposition temperature of PLA nanocomposites in both nitrogen and oxygen environments. The TGA and DTG curves of PLA nanocomposites recorded under nitrogen and oxygen atmospheres are shown in Fig. 5. The  $T_5$  refers to the decomposition temperature at 5% weight loss. The  $T_{d1}$  and  $T_{d2}$  indicate the first and second stage decomposition temperatures, respectively. It

**Fig. 4** TEM images of **a** PLA/HNT6/SEBS-g-MA5, **b** PLA/HNT6/SEBS-g-MA20, **c** PLA/HNT6/EBS5, and **d** PLA/HNT6/EBS20



**Table 3** TGA data of PLA nanocomposites under nitrogen and oxygen atmosphere

Material designation	Decomposition temperature (°C)					
	$T_5$		$T_{d1}$		$T_{d2}$	
	N <sub>2</sub> atm	O <sub>2</sub> atm	N <sub>2</sub> atm	O <sub>2</sub> atm	N <sub>2</sub> atm	O <sub>2</sub> atm
PLA	328.1	327.3	380.2	370.4	–	–
PLA/HNT6	311.5	313.7	374.2	366.5	–	–
SEBS-g-MA	424.0	296.5	–	396.2	508.0	522.5
PLA/HNT6/SEBS-g-MA5	320.5	316.0	371.0	359.3	492.2	431.4
PLA/HNT6/SEBS-g-MA20	326.1	310.5	374.8	365.1	499.0	479.5
EBS	298.5	279.5	436.6	362.2	–	–
PLA/HNT6/EBS5	293.5	302.0	336.7	368.6	–	435.4
PLA/HNT6/EBS20	293.8	295.2	328.9	360.5	–	458.3

**Fig. 5** TGA curves of PLA/HNT nanocomposites recorded under **a** nitrogen and **b** oxygen atmosphere; DTG curves of PLA/HNT nanocomposites recorded under **c** nitrogen and **d** oxygen atmosphere

was found that single-stage decomposition takes place in the nitrogen atmosphere, while a double-stage decomposition process occurred in the oxygen atmosphere. A double-stage decomposition process may relate to thermo-oxidation degradation. When a substance was combusted under oxidation atmosphere, it may undergo complex oxidation degradation process.

The decomposition of PLA at  $T_5$  is related to the random chain scission of PLA backbone chains. The  $T_5$  of PLA/HNT nanocomposites with 6 wt% HNT is lower than that of the

neat PLA. The free hydroxyl group on the HNT surface and the moisture entrapped within the tubular lumen of HNT could accelerate the thermal decomposition of PLA due to the dehydroxylation of hydroxyl group from HNT. The  $T_5$  of PLA and PLA/HNT nanocomposites were comparable both under nitrogen and oxygen atmosphere. Note that the  $T_{d1}$  of PLA and PLA/HNT nanocomposites is lower when the specimens were combusted under oxygen atmosphere. The presence of oxygen molecules could accelerate the oxidation degradation of polymer matrix. It can be observed



from Fig. 5c, d that the DTG curves of neat PLA give highest derivative weight under oxygen atmosphere. This indicates that the present of oxygen accelerate the degradation of polymer.

Two stages of decomposition were detected in PLA/HNT nanocomposites containing 20 wt% SEBS-g-MA. The second onset decomposition stage occurred at about 450 °C. This indicates that SEBS-g-MA has high thermal stability. However, the second stage of onset decomposition of PLA/HNT/SEBS-g-MA20 was shifted to a lower value of approximately 400 °C under oxygen atmosphere. From Table 3, reduction of  $T_5$  and  $T_{d1}$  of PLA/HNT/SEBS-g-MAH nanocomposites under oxidation atmosphere can be observed. Table 3 shows that the decomposition temperature (i.e.  $T_5$  and  $T_{d2}$ ) of SEBS-g-MA was shifted to lower decomposition temperature when SEBS-g-MA was undergoing thermo-oxidative degradation. This may be due to the polar MA group of SEBS, which are easily attacked by oxygen molecules at ambient temperature. It is believed that the formation of free radical in the specimens could accelerate the oxidation degradation. Thus, the PLA/HNT/SEBS-g-MA has lower thermal stability when combusted under oxygen compared to the one that under nitrogen condition.

Table 3 shows that in oxygen atmosphere, the  $T_5$  and  $T_{d1}$  of EBS are lower compared to those in a nitrogen atmosphere. This is because the thermo-oxidation degradation of EBS was initiated at the short hydrocarbon chain segment. Figure 3a, b shows the TGA curves of PLA/HNT nanocomposites (with and without EBS) recorded under nitrogen and oxygen atmosphere. The  $T_5$  and  $T_{d1}$  of PLA/HNT6/EBS5 and PLA/HNT6/EBS20 were shifted to higher temperatures under oxidation condition (c.f. Table 3). This may due to the -CONH in EBS enables the trapping of free radicals generated at higher combustion temperature [38].

### Differential Scanning Calorimetry (DSC)

Table 4 shows the thermal characteristics of PLA and PLA/HNT nanocomposites recorded from DSC. The glass

transition temperature for all PLA/HNT6 nanocomposites is approximately 58–61 °C. The neat PLA displayed two melting peaks i.e. 150.7 °C ( $T_{m,1}$ ) and 157.5 °C ( $T_{m,2}$ ). From Table 4, it can be seen that all of the PLA/HNT6 nanocomposites exhibited double melting endotherms. Double melting endotherms can be attributed to the melt re-crystallization mechanism of PLA which is originated from PLA crystal growth. The less perfect crystals ( $\alpha'$ -form crystal) of PLA have sufficient time to melt and reorganize into perfect crystals ( $\alpha$ -form crystals) before giving a second endotherm at higher temperature [39].

The  $T_{cc}$  of PLA was slightly shifted to a lower temperature from 113.5 to 109.0 °C by the incorporation of 6 wt% HNT. The  $\chi_c$  of PLA/HNT6 is about 31.3% which is slightly higher than that of PLA (29.9%). The shifting of  $T_{cc}$  of PLA to lower temperature could be attributed to the nucleating effects of HNT [40]. Note that, the addition of SEBS-g-MA into PLA/HNT6 nanocomposites shifted the  $T_{cc}$  (107–116 °C) to a higher temperature compared to that of PLA/HNT6 ( $T_{cc} = 109.0$  °C). The  $\chi_c$  of PLA/HNT6 nanocomposites decreased profoundly with further loading of SEBS-g-MA content. This indicates that SEBS-g-MA may retard the formation of large crystallites of PLA. According to Lim and Chow [41], the presence of rubber particles could act as physical hindrances towards crystal formation. Therefore, the growth of perfect lamellar crystals was limited. However, note that the  $T_{cc}$  of PLA/HNT/EBS nanocomposites are slightly lower compared to that of PLA/HNT6. According to Di et al. [42], PLA nanocomposites give a lower  $T_{cc}$  compared to that of PLA can be attributed to the nucleating effects of the well dispersed clay. It is interesting to note that the addition of EBS in PLA/HNT6 nanocomposites could remain the  $\chi_c$  (28–31%). This can be attributed to the fact that good dispersion HNT induced by EBS could eventually remain unchanged crystallisation process of PLA/HNT6.

**Table 4** Thermal characteristics of PLA and PLA/HNT nanocomposites recorded from DSC

Materials designation	$T_g$ (°C)	$T_{cc}$ (°C)	$T_{m,1}$ (°C)	$T_{m,2}$ (°C)	$T_c$ (°C)	$\chi_c$ (%)
PLA	58.7	113.5	150.7	157.5	–	29.9
PLA/HNT6	60.3	109.0	150.7	154.3	–	31.3
PLA/HNT6/SEBS-g-MA5	60.9	107.6	150.0	153.6	–	27.8
PLA/HNT6/SEBS-g-MA10	60.7	110.9	150.2	153.9	–	27.1
PLA/HNT6/SEBS-g-MA15	60.7	111.6	149.8	154.4	–	27.8
PLA/HNT6/SEBS-g-MA20	61.7	116.6	149.9	154.0	–	17.7
PLA/HNT6/EBS5	58.3	106.4	147.3	152.8	135.0	31.4
PLA/HNT6/EBS10	57.7	105.9	145.2	151.0	136.0	28.4
PLA/HNT6/EBS15	58.9	107.3	147.4	151.0	139.6	28.1
PLA/HNT6/EBS20	58.7	109.9	147.9	152.0	139.5	28.6



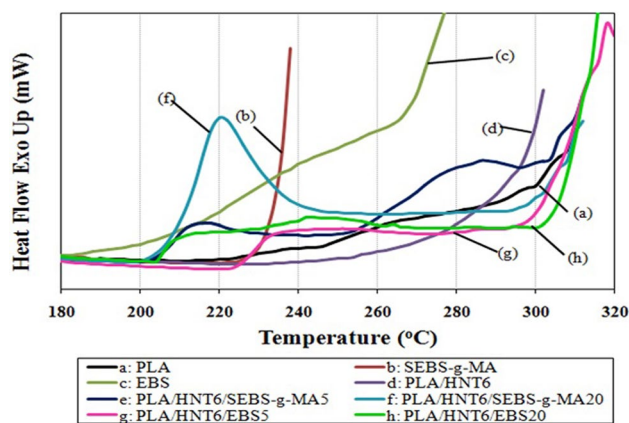


**Fig. 6** DSC curves of PLA/HNT6 nanocomposites (Note OOT was determined from the intercept point through the exothermic process of DSC curves)

**Table 5** OOT of PLA/HNT nanocomposites recorded from DSC

Material designation	OOT (°C)
PLA	221.2
PLA/HNT6	239.5
SEBS-g-MA	236.0
PLA/HNT6/SEBS-g-MA5	204.3
PLA/HNT6/SEBS-g-MA20	205.7
EBS	183.2
PLA/HNT6/EBS5	225.9
PLA/HNT6/EBS20	208.2

### Oxidation Onset Temperature (OOT)

Figure 6 shows the DSC curves of PLA/HNT6 nanocomposite and its OOT results are summarised in Table 5. The OOT of PLA was recorded at 221.2 °C. Adding 6 wt% of HNT shifted the OOT to higher temperatures at 239.5 °C. It is believed that the presence of HNT can increase the oxidation stability of PLA. The improvement in the oxidative stability was attributed to sorption effects caused by nanofiller, which hinders the diffusion of oxygen and restricts the volatilisation of decomposed gaseous from bulk polymer [43–45].

Table 5 shows that the OOT of SEBS-g-MA occurred at about 236 °C. The MA group of SEBS behave as catalysts of oxidation, favouring the formation of free radicals in the polymer matrix under an oxygen atmosphere. During the thermo-oxidative process, the MA hydrolysed to maleic acid at higher temperature. The maleic acid consists of acidic carboxylic group which acts as an active site inducing oxidation [46]. Adding of SEBS-g-MA in PLA/HNT6 nanocomposites activates thermal oxidation at early temperatures of approximately 198–210 °C due to the oxidation of MA group of SEBS. Table 5 shows that the OOT of EBS is approximately

183 °C. Although the OOT of EBS (183 °C) is lower than that of SEBS-g-MA (236 °C), note that the OOT of PLA/HNT6/EBS5 (225.9 °C) is higher than that of PLA/HNT6/SEBS-g-MA5 (204.3 °C).

### Conclusions

Based on this research devoted to study the effect of SEBS-g-MA and EBS on the mechanical, thermal and morphological properties of PLA/HNT nanocomposites, the following conclusions can be drawn.

The PLA/HNT6/EBS5 showed higher impact strength (98%) compared to that of PLA/HNT6/SEBS-g-MA5 (77%). The  $T_{cc}$  and  $\chi_c$  of PLA/HNT6 nanocomposites were influenced by the SEBS-g-MA and EBS content. The  $T_{cc}$  of PLA/HNT6 increased, while the  $\chi_c$  decreased as increasing of SEBS-g-MA content. On the other hand, the  $T_{cc}$  and  $\chi_c$  of PLA/HNT6/EBS is comparable to the PLA/HNT6 nanocomposites. From the TGA and OOT results, it can be revealed that the performance of SEBS-g-MA is sensitive to the oxygen atmosphere due to its MA group. Nevertheless, EBS could still perform in oxygen environment. As a conclusion, EBS can be a potential impact modifier for PLA/HNT nanocomposites, based on its improvement in impact strength, comparable  $T_{cc}$  and  $\chi_c$ , and it is less sensitive to the oxygen atmosphere as compared to SEBS-g-MA.

**Acknowledgements** This study was funded by Universiti Sains Malaysia Research University Grant (Grant Nos. 814070; 814199) and Ministry of Higher Education Malaysia MyPHD Scholarship Programme.

### References

1. Chow WS, Mohd Ishak ZA (2015) Polyamide blend-based nanocomposites: a review. *Express Polym Lett* 9:211–232
2. Liu X, Wu Q, Berglund LA (2002) Polymorphism in polyamide 66/clay nanocomposites. *Polymer* 43:4967–4972
3. Fu X, Qutubuddin S (2001) Polymer–clay nanocomposites: exfoliation of organophilic montmorillonite nanolayers in polystyrene. *Polymer* 42:807–813
4. Sinha Ray S, Yamada K, Okamoto M, Ogami A, Ueda K (2003) New polylactide/layered silicate nanocomposites. 3. High-performance biodegradable materials. *Chem Mater* 15:1456–1465
5. Yu L, Dean K, Li L (2006) Polymer blends and composites from renewable resources. *Prog Polym Sci* 31:576–602
6. Chun KS, Husseinsyah S (2014) Polylactic acid/corn cob eco-composites: effect of new organic coupling agent. *J Thermoplast Compos Mater* 27:1667–1678
7. Li Y, Han C, Bian J, Han L, Dong L, Gao G (2012) Rheology and biodegradation of polylactide/silica nanocomposites. *Polym Compos* 33:1719–1727
8. Cai YM, Lv JG, Feng JM (2013) Spectral characterization of four kinds of biodegradable plastics: poly(lactic acid), poly(butylene adipate-co-terephthalate), poly(hydroxybutyrate-co-hydroxyvalerate) and poly(butylene succinate) with FTIR and Raman Spectroscopy. *J Polym Environ* 21:108–114

9. Handge UA, Hedicke-Höchstötter K, Altstädt V (2010) Composites of polyamide 6 and silicate nanotubes of the mineral halloysite: influence of molecular weight on thermal, mechanical and rheological properties. *Polymer* 51:2690–2699
10. Dujkova Z, Merinska D, Slouf M (2013) Fire retardation of polystyrene/clay nanocomposites: initial study on synergy effect. *J Thermoplast Compos Mater* 26:1278–1286
11. Ismail H, Khoo WS, Ariffin A (2013) Effects of halloysite nanotubes and kaolin loading on the tensile, swelling, and oxidative degradation properties of poly(vinyl alcohol)/chitosan blends. *J Vinyl Addit Technol* 19:55–64
12. Lecouvet B, Bourbigot S, Sclavons M, Bailly C (2012) Kinetics of the thermal and thermo-oxidative degradation of polypropylene/halloysite nanocomposites. *Polym Degrad Stab* 97:1745–1754
13. Oburoğlu N, Ercan N, Durmus A, Kaşgöz A (2012) Effects of halloysite nanotube on the mechanical properties and nonisothermal crystallization kinetics of poly(butylene terephthalate)(PBT). *J Macromol Sci B Phys* 51:860–879
14. Rasal RM, Hirt DE (2008) Toughness decrease of PLA-PHBHHx blend films upon surface-confined photopolymerization. *J Biomed Mater Res A* 88A:1079–1086
15. Rasal RM, Janorkar AV, Hirt DE (2010) Poly(lactic acid) modifications. *Prog Polym Sci* 35:338–356
16. Noda I, Satkowski MM, Dowrey AE, Marcott C (2004) Polymer alloys of nodax copolymers and poly(lactic acid). *Macromol Biosci* 4:269–275
17. Wang YL, Hu X, Li H, Ji X, Li ZM (2010) Polyamide-6/poly(lactic acid) blends compatibilized by the maleic anhydride grafted polyethylene-octene elastomer. *Polym-Plast Technol Eng* 49:1241–1246
18. Zeng JB, Li YD, Zhu QY, Yang KK, Wang XL, Wang YZ (2009) A novel biodegradable multiblock poly(ester urethane) containing poly(L-lactic acid) and poly(butylenes succinate) blocks. *Polymer* 50:1178–1186
19. Tjong S, Xu S (2001) Ternary polymer composites: PA6,6/maleated SEBS/glass beads. *J Appl Polym Sci* 81:3231–3237
20. Švab I, Musil V, Šmit I, Makarovič M (2007) Mechanical properties of wollastonite-reinforced polypropylene composites modified with SEBS and SEBS-g-MA elastomers. *Polym Eng Sci* 47:1873–1880
21. Liu SP, Ying JR, Zhou XP, Xie XL, Mai YM (2009) Dispersion, thermal and mechanical properties of polypropylene/magnesium hydroxide nanocomposites compatibilized by SEBS-g-MAH. *Compos Sci Technol* 69:1873–1879
22. Denac M, Musil V, Šmit I (2005) Polypropylene/talc/SEBS (SEBS-g-MA) composites. Part 2. Mechanical properties. *Compos A Appl Sci Manuf* 36:1282–1290
23. Kusmono, Mohd Ishak ZA, Chow WS, Takeichi T, Rochmadi (2008) Compatibilizing effect of SEBS-g-MA on the mechanical properties of different types of OMMT filled polyamide 6/polypropylene nanocomposites. *Compos A Appl Sci Manuf* 39:1802–1814
24. Tjong SC, Xu SA, Mai YM (2003) Tensile deformation mechanism of polyamide 6, 6/SEBS-g-MA blend and its hybrid composites reinforced with short glass fibers. *J Mater Sci* 38:207–215 (2003)
25. Yemele MCN, Koubaa A, Cloutier A, Soulounganga P, Wolcott M (2010) Effect of bark fiber content and size on the mechanical properties of bark/HDPE composites. *Compos A Appl Sci Manuf* 41:131–137
26. Li T, Wolcott M (2006) Rheology of wood plastics melt, part 2: effects of lubricating systems in HDPE/maple composites. *Polym Eng Sci* 46:464–473
27. Kiatkamjornwong S, Thakeow P, Sonsuk M (2001) Chemical modification of cassava starch for degradable polyethylene sheets. *Polym Degrad Stab* 73:363–375
28. Yang Z, Zhou C, Yang H, Cai T, Cai J, Li HB, Zhou D, Chen BF, Li AM, Cheng RS (2012) Improvement of the compatibilization of high-impact polystyrene/magnesium hydroxide composites with partially sulfonated polystyrene as macromolecular compatibilizers. *Ind Eng Chem Res* 5:9204–9212
29. Yu ZF, Yang YY, Zhang LL, Ding YC, Chen XM, Xu KT (2012) Study of short glass fiber-reinforced poly(3-hydroxybutyrate-co-4-hydroxybutyrate) composites. *J Appl Polym Sci* 126:822–829
30. Ndazi BS, Karlsson S (2011) Characterization of hydrolytic degradation of polylactic acid/rice hulls composites in water at different temperatures. *Express Polym Lett* 5:119–131
31. Mohapatra AK, Mohanty S, Nayak SK (2012) Poly(lactic acid) and layered silicate nanocomposites prepared by melt mixing: thermomechanical and morphological properties. *Polym Compos* 33:2095–2104
32. Chow WS, Lim SR (2013) Effects of N,N'-ethylenebis (stearamide) on the properties of poly (ethylene terephthalate)/organomontmorillonite nanocomposite. *Polym Plast Technol Eng* 52:626–633
33. Tjong SC, Bao SP (2007) Fracture toughness of high density polyethylene/SEBS-g-MA/montmorillonite nanocomposites. *Compos Sci Tech* 67:314–323
34. Kusmono, Mohd Ishak ZA, Chow WS, Takeichi T (2008) Influence of SEBS-g-MA on morphology, mechanical, and thermal properties of PA6/PP/organoclay nanocomposites. *Eur Polym J* 44:1023–1039
35. Lin Y, Chen H, Chan CM, Wu J (2010) The toughening mechanism of polypropylene/calcium carbonate nanocomposites. *Polymer* 2010 51:3277–3284
36. Bartczak Z, Argon AS, Cohen RE, Weinberg M (1999) Toughness mechanism in semi-crystalline polymer blends: II. High-density polyethylene toughened with calcium carbonate filler particles. *Polymer* 40:2347–2365
37. Alhuthali A, Low IM (2013) Mechanical and fracture properties of halloysite nanotube reinforced vinyl-ester nanocomposites. *J Appl Polym Sci* 130:1716–1725
38. Cerrutia P, Carfagnaa C, Rychly J, Matisova-Rychla L (2003) Chemiluminescence from oxidation of polyamide 6,6. I. The oxidation of pure polyamide. *Polym Degrad Stab* 82:477–485
39. Tham WL, Poh BT, Mohd Ishak ZA, Chow WS (2014) Thermal behaviors and mechanical properties of halloysite nanotube-reinforced poly(lactic acid) nanocomposites. *J Therm Anal Calorim* 118:1639–1647
40. Tham WL, Poh BT, Mohd Ishak ZA, Chow WS (2016) Epoxidized natural rubber toughened poly(lactic acid)/halloysite nanocomposites with high activation energy of water diffusion. *J Appl Polym Sci* 42850
41. Lim SR, Chow WS (2012) Impact, thermal, and morphological properties of functionalized rubber toughened-poly (ethylene terephthalate) nanocomposites. *J Appl Polym Sci* 123:3173–3181
42. Di Y, Iannace S, Maio ED, Nicolais L (2005) Poly (lactic acid)/organoclay nanocomposites: thermal, rheological properties and foam processing. *J Polym Sci B Polym Phys* 43:689–698
43. Bertini F, Canetti M, Audisio G, Costa G, Falqui L (2006) Characterization and thermal degradation of polypropylene/montmorillonite nanocomposites. *Polym Degrad Stab* 91:600–605
44. Khumalo VM, Karger-Kocsis J, Thomann R (2010) Polyethylene/synthetic boehmite alumina nanocomposites: structure, thermal and rheological properties. *Express Polym Lett* 4:264–274
45. Dominkovics Z, Hári J, Fekete E, Pukánszky B (2011) Thermo-oxidative stability of polypropylene/layered silicate nanocomposites. *Polym Degrad Stab* 96:581–587
46. Tidjani A, Wald O, Pohl MM, Hentschel MP, Schartel B (2003) Polypropylene-graft-maleic anhydride-nanocomposites: I. Characterization and thermal stability of nanocomposites produced under nitrogen and in air. *Polym Degrad Stab* 82:133–140